

## A global topographic map of Titan

Ralph D. Lorenz<sup>a,\*</sup>, Bryan W. Stiles<sup>b</sup>, Oded Aharonson<sup>c</sup>, Antoine Lucas<sup>d</sup>, Alexander G. Hayes<sup>e</sup>, Randolph L. Kirk<sup>f</sup>, Howard A. Zebker<sup>g</sup>, Elizabeth P. Turtle<sup>a</sup>, Catherine D. Neish<sup>h</sup>, Ellen R. Stofan<sup>i</sup>, Jason W. Barnes<sup>j</sup>, the Cassini RADAR Team

<sup>a</sup>Space Department, Johns Hopkins University Applied Physics Laboratory, 11100 Johns Hopkins Road, Laurel, MD 20723, USA

<sup>b</sup>Jet Propulsion Laboratory, California Institute of Technology, Pasadena, CA 91109, USA

<sup>c</sup>Helen Kimmel Center for Planetary Science, Weizmann Institute of Science, Rehovot 76100, Israel

<sup>d</sup>Laboratoire AIM, Université Paris 7/CNRS/CEA, 91191 Gif sur Yvette Cedex, France

<sup>e</sup>Cornell University, Ithaca, NY 14853, USA

<sup>f</sup>U.S. Geological Survey, Flagstaff, AZ 86001, USA

<sup>g</sup>Department of Electrical Engineering, Stanford University, Stanford, CA 94305, USA

<sup>h</sup>Goddard Space Flight Center, Greenbelt, MD 20771, USA

<sup>i</sup>Proxemy Research, Rectortown, VA 20140, USA

<sup>j</sup>University of Idaho, Moscow, ID 83844, USA

### ARTICLE INFO

#### Article history:

Received 29 January 2013

Revised 27 March 2013

Accepted 2 April 2013

Available online 18 April 2013

#### Keywords:

Titan

Geological processes

### ABSTRACT

Cassini RADAR SARTopo and altimetry data are used to construct a global gridded  $1 \times 1^\circ$  elevation map, for use in Global Circulation Models, hydrological models and correlative studies. The data are sparse, and so most of the map domain ( $\sim 90\%$ ) is populated with interpolated values using a spline algorithm. The highest ( $\sim +520$  m) gridded point observed is at  $48^\circ\text{S}$ ,  $12^\circ\text{W}$ . The lowest point observed ( $\sim 1700$  m below a 2575 km sphere) is at  $59^\circ\text{S}$ ,  $317^\circ\text{W}$ : this may be a basin where liquids presently in the north could have resided in the past. If the deepest point were once a sea with the areal extent of present-day Ligeia Mare, it would be  $\sim 1000$  m deep. We find four prominent topographic rises, each  $\sim 200$  km wide, radar-bright and heavily dissected, distributed over a  $\sim 3000$  km arc in the southeastern quadrant of Titan ( $\sim 40\text{--}60^\circ\text{S}$ ,  $15\text{--}150^\circ\text{W}$ ).

© 2013 Elsevier Inc. All rights reserved.

### 1. Introduction

Many geological, hydrological and meteorological processes are profoundly affected by topography. To fully understand these processes it is desirable to have a global topographic dataset of high and uniform horizontal and vertical resolution: Mars science was revolutionized by the generation of such data by the laser altimeter instrument MOLA, and lunar science is currently benefiting from the data being generated by the Lunar Orbiter Laser Altimeter (LOLA).

Titan displays a range of fascinating and dramatic meteorological and other processes that are evidently affected by topography on various scales. For example, Lorenz et al. (2008) observed that even an early (and highly incomplete) sampling of Titan's river channels suggested a generally poleward trend in flow direction, which is consistent with initial topography data that showed that the poles are topographically lower than the equator (Zebker et al., 2009a). Lorenz and Radebaugh (2009) showed that the equatorial linear dunes are diverted by topographic highs of 100–300 m with

slopes of the order of 1/200, but blocked by slopes of 1/50 or more. It is therefore a pity that our knowledge of Titan's topography is and will remain very poor compared with Earth, Mars, Venus and the Moon, where global maps exist. For Titan, such a global dataset must await a future Titan orbiter mission, and radar altimeters have been suggested as priority instruments for such a mission.

While far from global in extent, nor uniform in quality, Cassini radar topography data are now sufficient to assemble a useful topography map at fairly high resolution. Using a smaller subset of these data, Zebker et al. (2009a) determined the low-order shape of Titan's surface with a spherical harmonic analysis, and Lorenz et al. (2011) evaluated Titan's hypsogram. The utility of maps developed from sparse data at Mars was demonstrated pre-MOLA by Smith and Zuber (1996) who studied Mars' shape using a limited number of Viking orbiter radio occultation heights and groundbased radar tracks and determined the character of the north–south dichotomy (see also Aharonson et al., 2001).

Recent applications of topography data (which have used the Zebker et al. (2009a) spherical harmonic solutions) include the effects on winds in a Global Circulation Model (GCM) by Tokano (2010) and the examination of the spatial extent of liquids on Titan as a function of ocean volume (Larsson and McKay (2013)). Efforts

\* Corresponding author.

E-mail address: [ralph.lorenz@jhuapl.edu](mailto:ralph.lorenz@jhuapl.edu) (R.D. Lorenz).

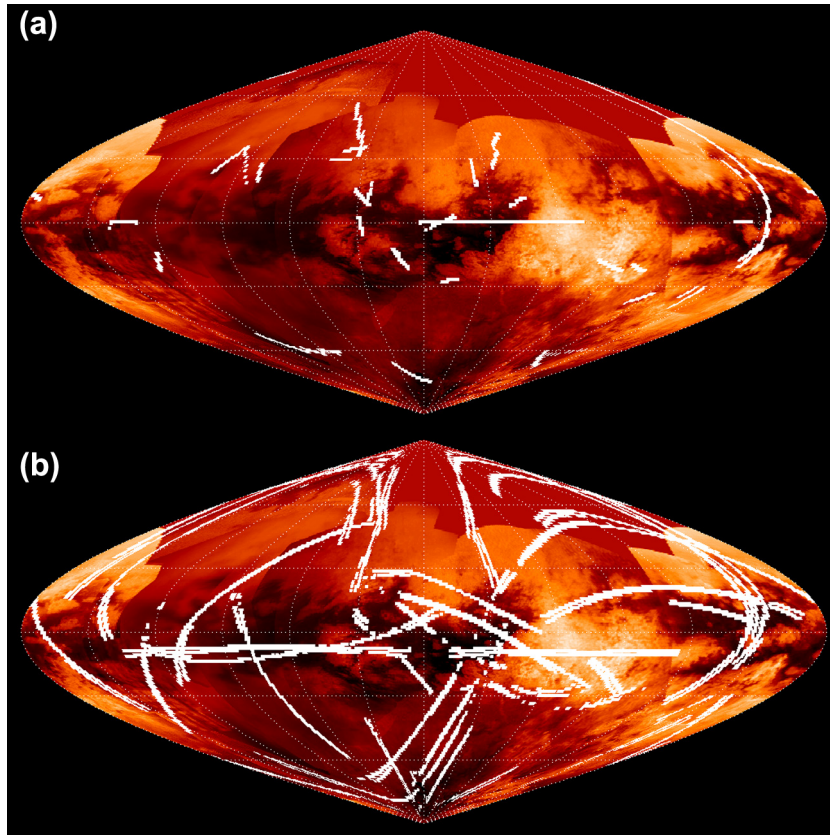


**Fig. 1.** Topography data coverage on a sinusoidally projected 940 nm albedo map of Titan, centered on the 180° meridian. (a) Altimetry swaths – note the T77 swath along the equator just right of center, and the long T30 swath at the upper right edge. (b) The much more extensive SARtopo coverage.

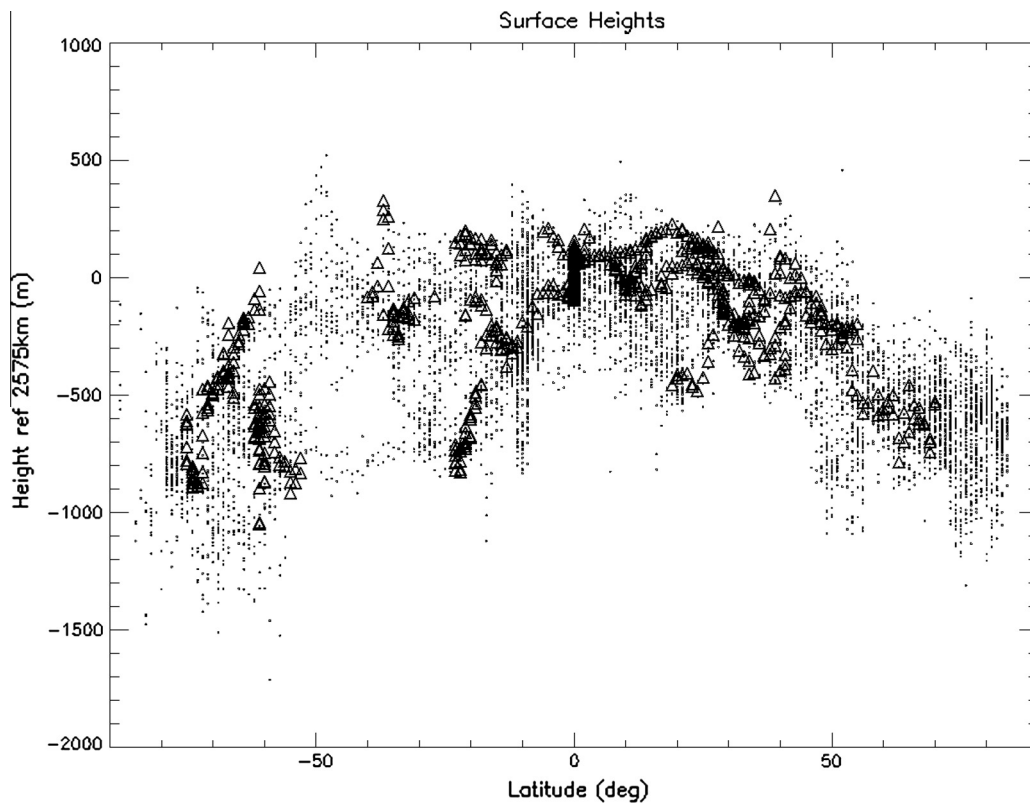


**Fig. 2.** Surface heights in  $1 \times 1^\circ$  bins from SARtopo (small circles) and altimetry (triangles). Both datasets show the oblateness of Titan. (Cf. profiles along lines of latitude in Fig. 5 and longitude in Fig. 6.)

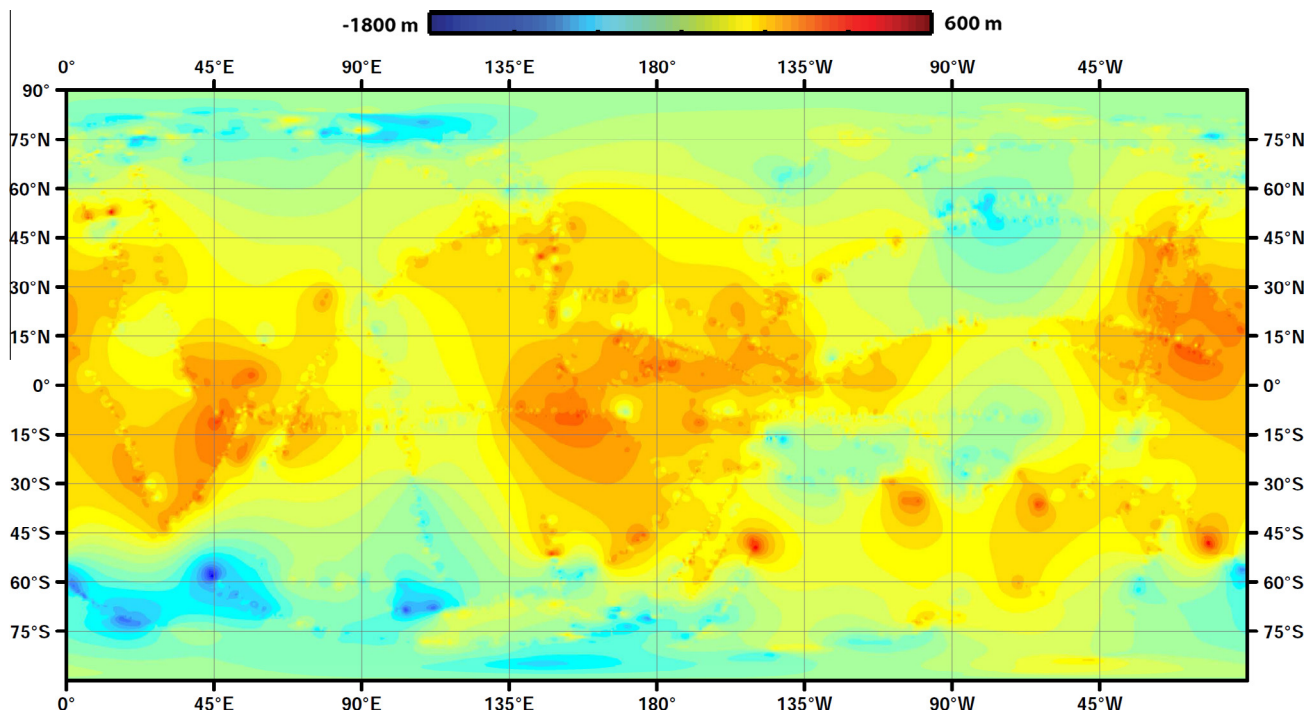


**Fig. 3.** Interpolated topography. These data are in [Supplementary Data file #1](#), and are plotted with contours in [Fig. 9](#). The influence of the original data can be seen in some changes of slope, and that large areas are present where no short-wavelength topography is seen (because there are no data to indicate it).

such as these can benefit from a higher-resolution topography product. Thus we offer here a documented topographic map product in a convenient form. The product is definitive in that it captures the data available at present and only a few tracks per year will be added subsequently: it may be that no significant update is worthwhile until the completion of the Cassini Solstice Mission in 2017. The map product is available for download in digital form as [Supplemental information](#) and at <http://www.lpl.arizona.edu/~rlorenz/topomap.html> and may additionally be archived in future at the NASA Planetary Data System (PDS).

We offer in this paper only some brief interpretations and observations about the topographic map. Correlative studies with broader datasets and geophysical analyses of topography are left for future work in the interests of making the present data available promptly.

## 2. Titan topographic data

Available topographic data on Titan is discussed at some length in [Lorenz et al. \(2011\)](#). The principal data source here is the synthetic aperture radar (SAR) imaging, which covers approximately 35% of Titan's surface with narrow swaths a couple of hundred km wide. An along-track topographic estimate profile, named SARTopo, can be generated by exploiting the overlap in the beam footprints used to generate the swath to estimate the terrain height in several bands along the length of the swath ([Stiles et al., 2009](#)). Note that high-altitude single-beam SAR imaging has been used to extend the imaging coverage of Titan, but since it has no overlapping beams, provides no direct topography. The dataset presented here is rather more extensive than that used in the construction of Titan's hypsogram in [Lorenz et al. \(2011\)](#) in so far as that study used only the SARTopo dataset for flybys TA-T61. The present dataset through T65 comprises 132 SARTopo tracks (for each SAR imaging flyby, there are typically three different topography swaths between the different beam pairs.) Although

the posting of individual heights is made quite closely, such that the dataset comprises about 1.3 million datapoints, there is partial overlap between the  $\sim 20$  km wide correlation regions used and so the profiles are oversampled.

Additionally, radar altimetry along 20 short tracks ( $\sim 300$ – $700$  km long, [Zebker et al., 2009b](#)) has been obtained, plus three long ones: T30, 3600 km from high northern latitudes down to the equator near the prime meridian, T49 across Ontario Lacus (e.g. [Wye et al., 2009](#)), and T77 along the equator at the Shangri-La/Xanadu boundary. An additional long altimetry swath was acquired by the spacecraft on T60 in August 2009 but was lost due to a Deep Space Network antenna outage. The 23 altimetry tracks through T77 are used, which introduce another  $\sim 12,000$  datapoints. These data are available via the NASA Planetary Data system as 'Altimeter Summary Files', e.g. 'T77\_ABDR\_SUMMARY\_04\_D229\_V02.CSV'. The SARTopo data is presently being validated for general use (and indeed during the preparation of this paper, we identified some spurious points in preliminary SARTopo files). Note that we use the 'Corrected First Moment' (or corrected centroid) height estimate, as this is most consistent with the SARTopo heights – see [Zebker et al. \(2009b\)](#) for further discussion. Also note that these data include a few points with unphysical surface heights that were acquired when the spacecraft attitude deviated from nadir during flyby T41 – these points can be excluded by requiring the incidence angle for valid data to be less than  $0.7^\circ$ .

The geographical distributions of the two datasets are presented in [Fig. 1](#). By design, there are no major unobserved regions on a hemispheric scale, although some gaps  $\sim 60^\circ$  ( $\sim 2000$  km) across are unavoidably present due to the distribution of Cassini orbits. When the data are binned in  $1^\circ \times 1^\circ$  latitude–longitude space, the SARTopo data fill 6696 of the 64,800 bins (compared with 5400 in [Lorenz et al., 2011](#)) and the altimetry adds an additional 770 bins. By this metric, topography data, corresponding to of order 100,000 km of tracks, covers about 11% of Titan's surface.

The binned data are plotted in [Fig. 2](#) against latitude. The depression of Titan's poles (e.g. [Zebker et al., 2009a, 2009b](#)) is

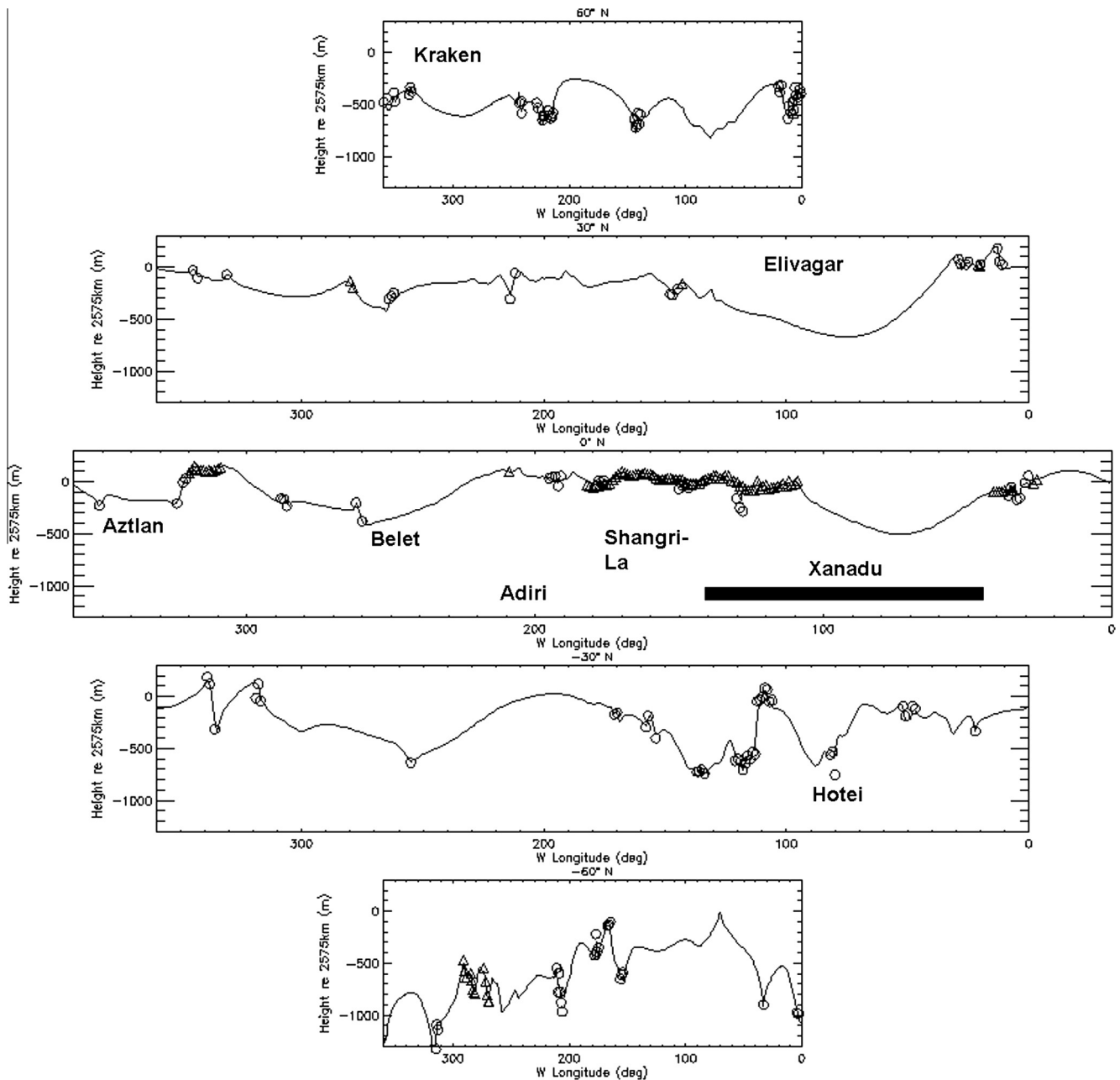


**Fig. 4.** Surface height profiles along lines of latitude. The length of the plots is scaled such that the physical length scale is the same (the latitude circle at 60° north or south is half of the 16,180 km length at the equator). The solid line is the interpolated topography field, circles denote SARTopo measurements and triangles show altimetry measurements. Titan's prolate shape is evident as a wavenumber-2 variation with longitude, most prominent at 30°N and at the equator, with local maxima near the prime meridian.

clearly seen in both datasets. It is not surprising that the two datasets are generally consistent with each other in that the SARTopo data have been controlled to available altimeter points.

It is of interest to note the extreme values in these data. The highest bin in the altimeter data is at 216°W, 39°N, at 352 m, while in the SARTopo it is found at 12°W 48°S, at 520 m (note that there is no overlapping altimetry data here for comparison). The minimum elevations found are at 258°W, 61°S (−1049 m, altimetry) and 316°W, 59°S (−1712 m, SARTopo). Since the SARTopo data are more extensive, it is not surprising that the most extreme values are found in those data. It is noteworthy that the lowest point measured is deep in the southern hemisphere. Note that these are not the extreme values in the original datasets, but are the extreme

values of the  $1 \times 1^\circ$  averages, so isolated and small higher and lower points may exist even in the observed areas.

### 3. Interpolation scheme

In order to fully populate a map grid, we must interpolate those values where measurements are not present. This is a well-known problem in geophysics, geology and other fields. For the present application, following other geological gridding analyses, we employ the spline technique with tension, which minimizes curvature while maintaining continuous second derivatives (Smith and Wessel, 1990). This approach also avoids the issue that spherical harmonic approaches can insert features where there are no data

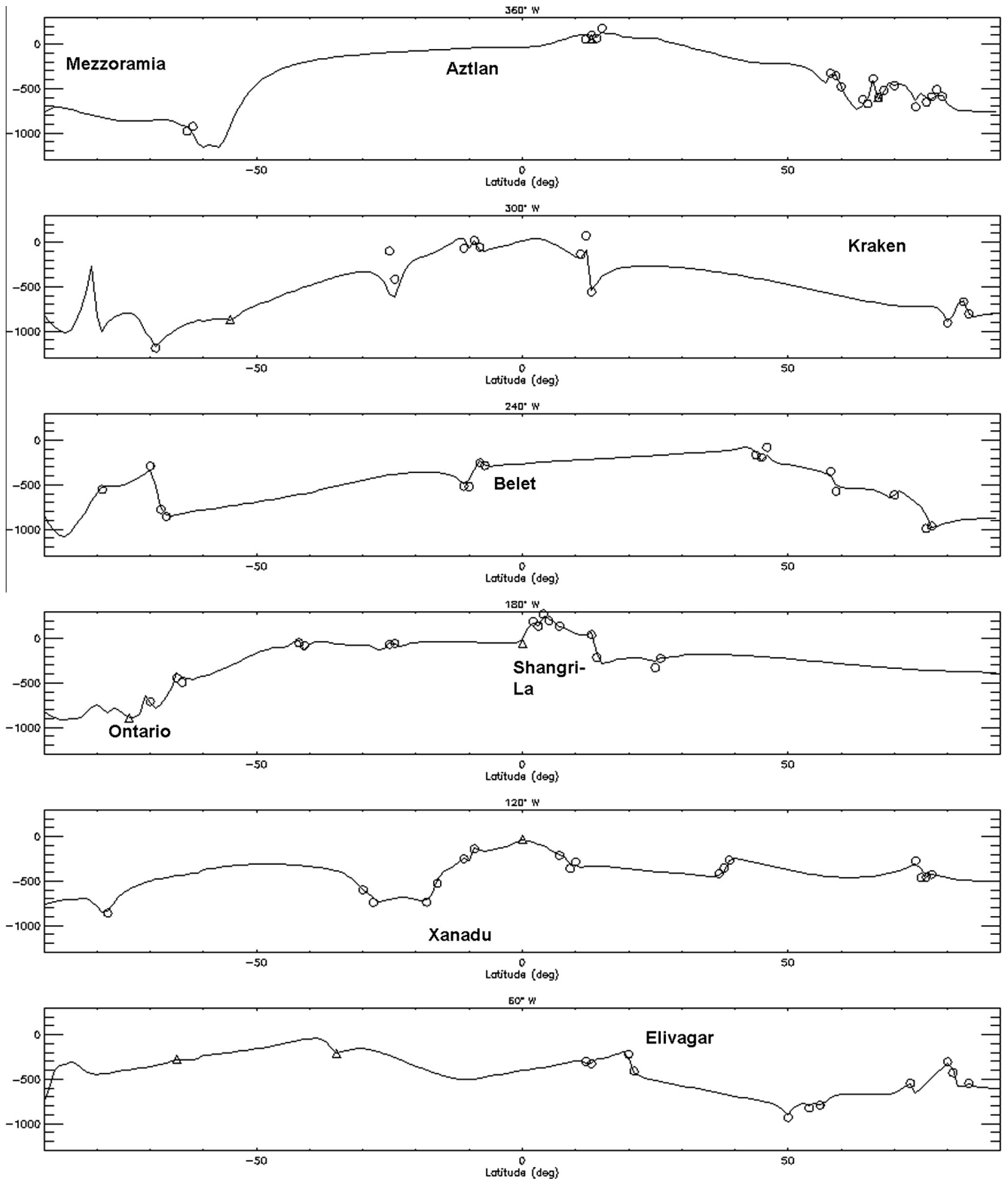
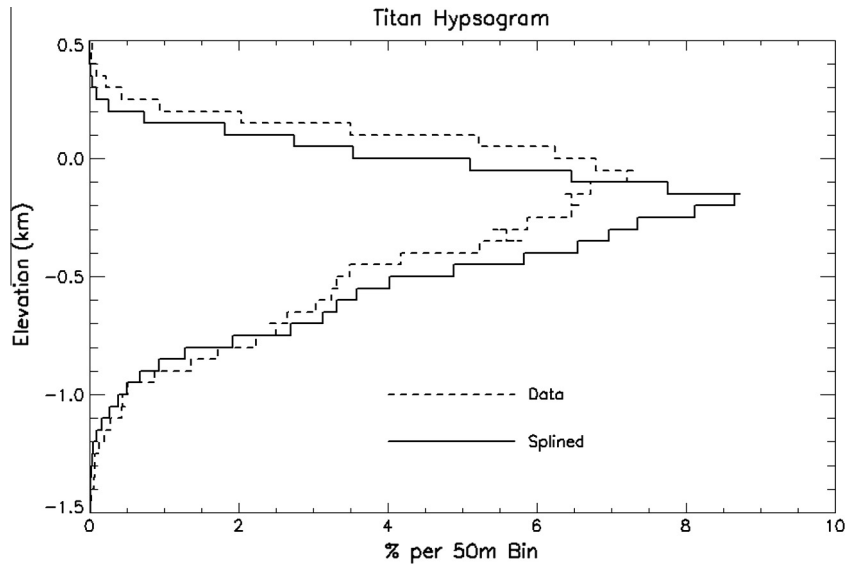


Fig. 5. As for Fig. 4, but profiles along meridians from the south pole at left to north pole at right. Titan's polar depressions are particularly evident at the prime meridian.

(e.g. antipodal to large features that are observed). The splining (with tension = 0.5) is performed twice, once with conventional cylindrical coordinates, and once with coordinates rotated 90°, such that interpolations across the poles are well-behaved and the two grids blended accordingly. The resulting field (Fig. 3) is seen to have smooth behavior where there is no data and joins points reasonably.

We confirmed that this approach was robust by comparing with a somewhat heuristic approach of averaging across all azimuths from a point. For the point to be estimated, the data grid is searched in each of 32 equispaced directions until height data is found (or a distance of 60° is exceeded). From this set of up to 32 points, the height estimate is computed by weighting each point by its distance raised to an exponent  $-2$ . This conceptually



**Fig. 6.** Hypsogram of the source data, and of the splined map. The splined map is narrower, by definition, since it contains many interpolated values.

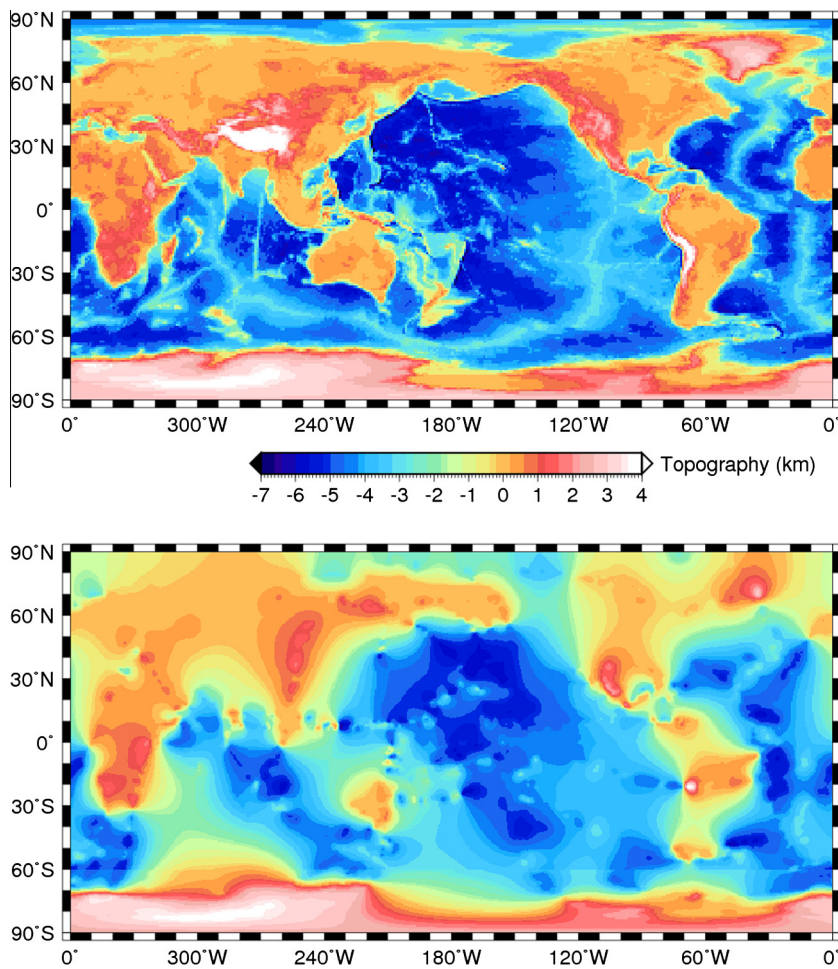


**Fig. 7.** A cylindrical map of Earth topography. Top panel is the full dataset (at  $0.5 \times 0.5^\circ$  resolution) whereas the lower panel is the estimated topography field obtained by downsampling to  $1 \times 1^\circ$ , extracting data from that grid at those coordinates where we have Titan data, and performing the spline interpolation as described in the text. The major ocean basins and continental land masses (including Greenland and Australia) are identified, together with major mountainous regions (with the exception of the Tibetan plateau, which did not happen to lie on a data take).

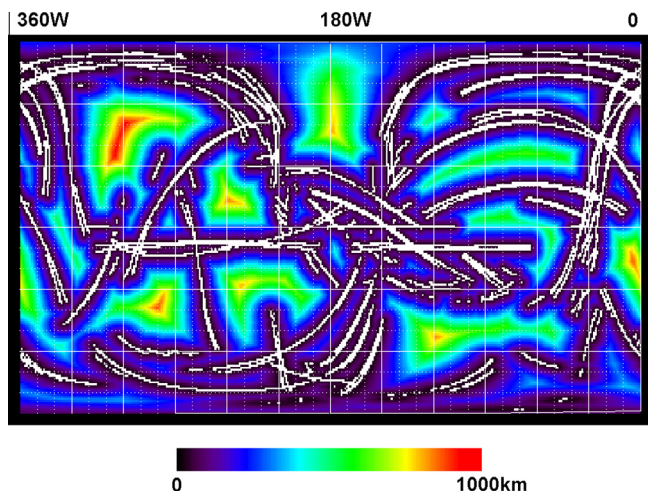


**Fig. 8.** Distance to the nearest measured height. The cylindrical projection is the same as for other maps. These data are in Supplemental Data file #2.

simple approach yields a broadly similar result, confirming the robustness of the major features in the grid, but has poor polar appearance and a few faint artifacts (see Supplementary Fig. 1). Alternative choices of exponent, or different tension values in the splining method, yield substantially similar results.

The rms difference between the chosen (splined  $T = 0.5$ ) dataset and the original data is about 30 m: this compares with the estimated accuracy of the original data of typically 100 m or so (Stiles et al., 2009; Zebker et al., 2009b). No attempt has been made to apply error-determined weights to the gridding procedure.

The map data are provided as an array of numbers in Supplemental Data file #1. Profiles through the interpolated map are shown in Figs. 4 and 5: this shows how the interpolation scheme introduces steep slopes where they are required to agree with the data, and otherwise smoothly joins the points. Fig. 6 shows a hypsogram of the interpolated map, and of the original data – it is seen that they are similar, although (as one might expect) the interpolated distribution is slightly narrower since by definition it includes points that are intermediate to the original data.

Fig. 7 shows a topographic map of the Earth at  $1 \times 1^\circ$  resolution, using the GTOPO5 dataset, and the corresponding map obtained by sampling that data with the same geographical distribution of points as we have available for Titan, and then applying our spline interpolation procedure. This then gives a qualitative impression of how well the data at hand captures the global topographic characteristics of a planet (a related exercise by Lorenz (1996) showed that recognition of a partly-observed landscape improves sharply up to  $\sim 30\%$  coverage, with the incremental value of additional coverage only decreasing above that point). It is seen that while some extremes are not captured the overall shape of the continental land masses (including Greenland and Australia) is identified, together with major mountainous regions (with the exception of the Tibetan plateau). Supplemental Fig. 2 shows the results of the same exercise for Mars.

Fig. 8 indicates the distance in the map to the nearest measurement (provided as a cylindrical map to facilitate lookup of specific coordinates). This map (provided as Supplemental Data file #2) can serve as a guide for interpretive analyses – clearly one should exercise caution when drawing conclusions about topography for areas distant from where there is actual data. The largest distance is about 1000 km (equivalent to  $\sim 20^\circ$  of latitude along a meridian, or  $20^\circ$  of longitude at the equator); some of these largest gaps may be partly filled by planned future data acquisitions.

## 4. Maps and geological discussion

The map from Fig. 3 is shown with contours added to facilitate the indication of slope directions in Fig. 9, together with a VIMS basemap and the original data tracks for reference. The polar regions are shown in stereographic projection in Fig. 10.

The maps, and the data file in Supplemental information, are given as surface heights relative to a 2575 km sphere, and thus are suitable for purely geometric work (e.g. occultation timing). For problems relating to gravity, such as hydrology, the ellipsoidal geoid of less et al., 2010 should be subtracted to get heights relative to an equipotential. Since the geoid amplitude is only  $\sim 100$  m equator-to-pole, the effects in many cases will not be significant, however.

Note that no attempt has been made to force the present topography dataset to be flat in Titan's seas. This is in part to expose the original data (which might afford some insight into how deep the basins might be expected to be), and because the complete extent of Kraken Mare has not yet been determined in radar data, so any attempt to flatten the seas would be somewhat subjective.

The fact that Titan's topographic range is only about 2.5 km has been noted previously (Lorenz et al., 2011). That paper also noted that the hypsogram appeared negatively skewed, with some exceptional troughs. The map highlights at least one of these (see Section 4.2).

### 4.1. Overall pattern

The most striking impression overall is that of two equatorial highland provinces, somewhat near the sub- and anti-saturnian points ( $0^\circ$  and  $180^\circ$ W, respectively). These were apparent as a prolateness of Titan's figure (Zebker et al., 2009b), in other words a  $C_{22}$  topography term. This topographic bulge is rather in excess of Titan's measured geoid (less et al., 2010) and indeed larger than the  $\sim 100$  m tidal bulge that would be expected from hydrostatic equilibrium. The relationship of the long-wavelength topographic variation on Titan to the gravity field is discussed in Nimmo and Bills (2010) who infer a non-convecting ice crust with a thickness that varies with latitude.

Two complex highland regions can be seen spanning the equatorial region. These highland terrains are irregular, with significant entrant depressions and outlying hills. A striking aspect, and one that is a reversal of the common association of optically bright with radar-bright and locally elevated terrain, is that at the large scale, there is a poor correlation of albedo and elevation. While some sand seas like Belet and Fensal are in depressions, others (Shangri-La) are not. Conversely, the southern portion of the well-known bright region Xanadu (Radebaugh et al., 2011) is partly a depression, but is not filled with sand.

The variation in topography across Xanadu from north to south (Figs. 5 and 9) is intriguing (and inconsistent with the interpretation of the western part of Xanadu as having an impact origin (Brown et al., 2011) unless there has been a significant and asymmetric post-formation change in topography). It is, perhaps, interesting that Hotei and Tui Regios which have been suggested to have cryovolcanic origins (e.g. Wall et al., 2009; Lopes et al., 2013) both lie within the lower elevation portion of Xanadu. An alternative proposal, consistent with this lower elevation, has been that Tui and especially Hotei are former lake beds, as evidenced by drainage patterns (e.g. Moore and Howard, 2010) and a spectral signature seen elsewhere in lake margins and interpreted to indicate evaporite deposits (Barnes et al., 2011). The contiguous nature of the dune fields from Fensal/Aztlan through Senkyo and Belet and around Adiri to Shangri-La clearly demonstrates that, as expected,

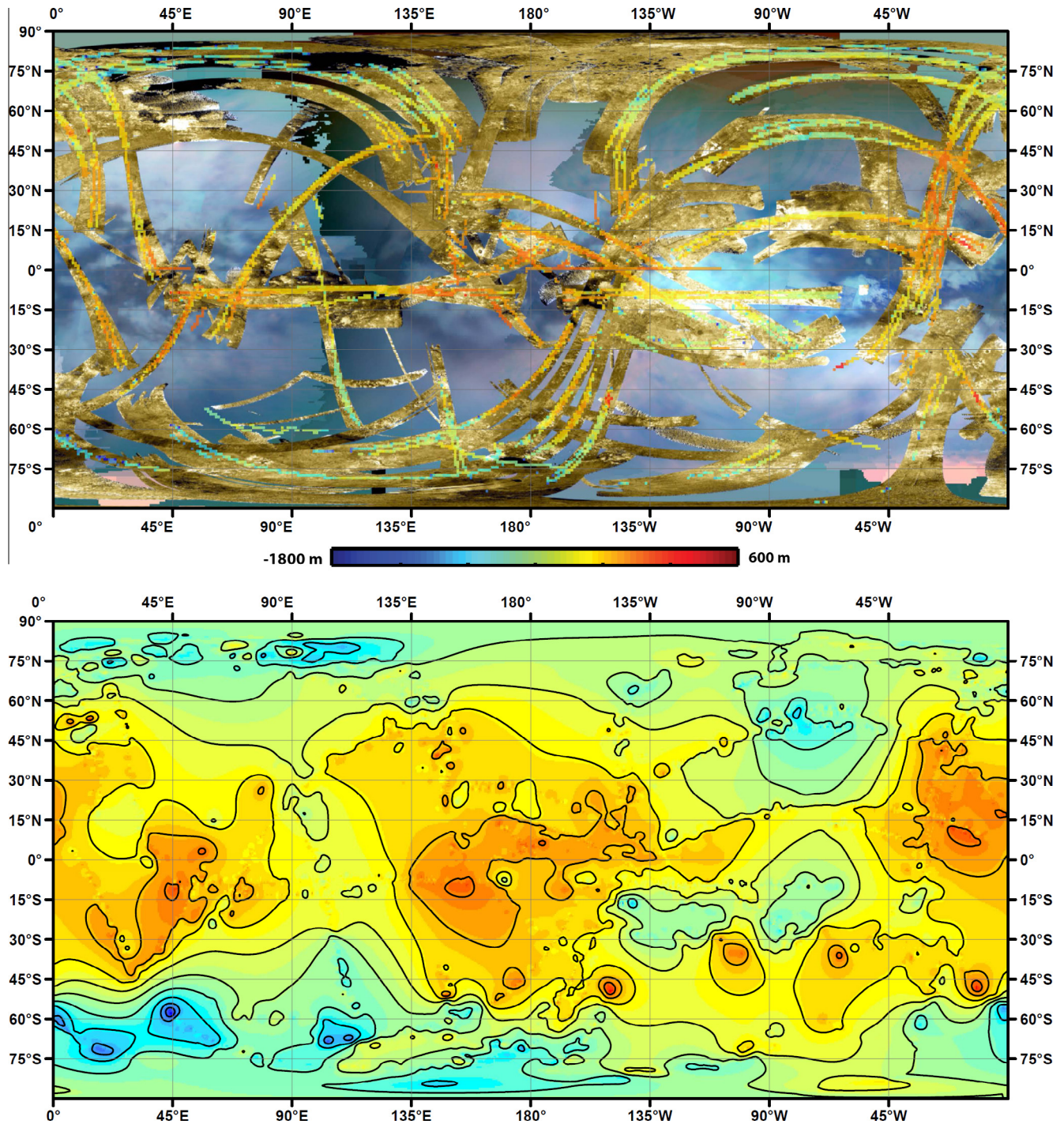


**Fig. 9.** Cylindrical maps. Upper panel is a VIMS multispectral basemap with gold-colored radar imaging where coverage exists and color-coded topography where that data are present. The lower panel shows the same interpolated topography field as Fig. 3, but with 200 m contours added to facilitate interpretation. The south polar depressions, and four mountains (see Fig. 11) are notably prominent. A dark region at 50–65°S, 300–360°W coincides with a major depression. It is striking that there is in fact an anticorrelation with albedo at the largest scales, wherein some sand seas are not in large depressions but are most extensive at the pro- and anti-saturnward bulges. (For interpretation of the references to color in this figure legend, the reader is referred to the web version of this article.)

while dunes are interrupted (deflected or truncated) by short-wavelength changes in topography (even if the change in elevation is low) they are not affected by even large changes in elevation over long distances, i.e. low slopes.

As the profiles show (Figs. 4 and 5), steep slopes, and sudden changes in slope, are often encountered. We defer, however, analyses of slope statistics and spectral analysis of topography to future work.

#### 4.2. Basins for southern seas?

Stofan et al. (2012) have proposed in SAR image data some morphological evidence for wide basins that may be the vestige of prior seas. The concentration of lakes and seas in the north polar region is a remarkable contrast with the south, but seems likely to be an ephemeral situation: the timescale for Croll–Milankovich climate cycles on Titan is  $\sim 50,000$  years (Aharanson et al., 2009) and thus

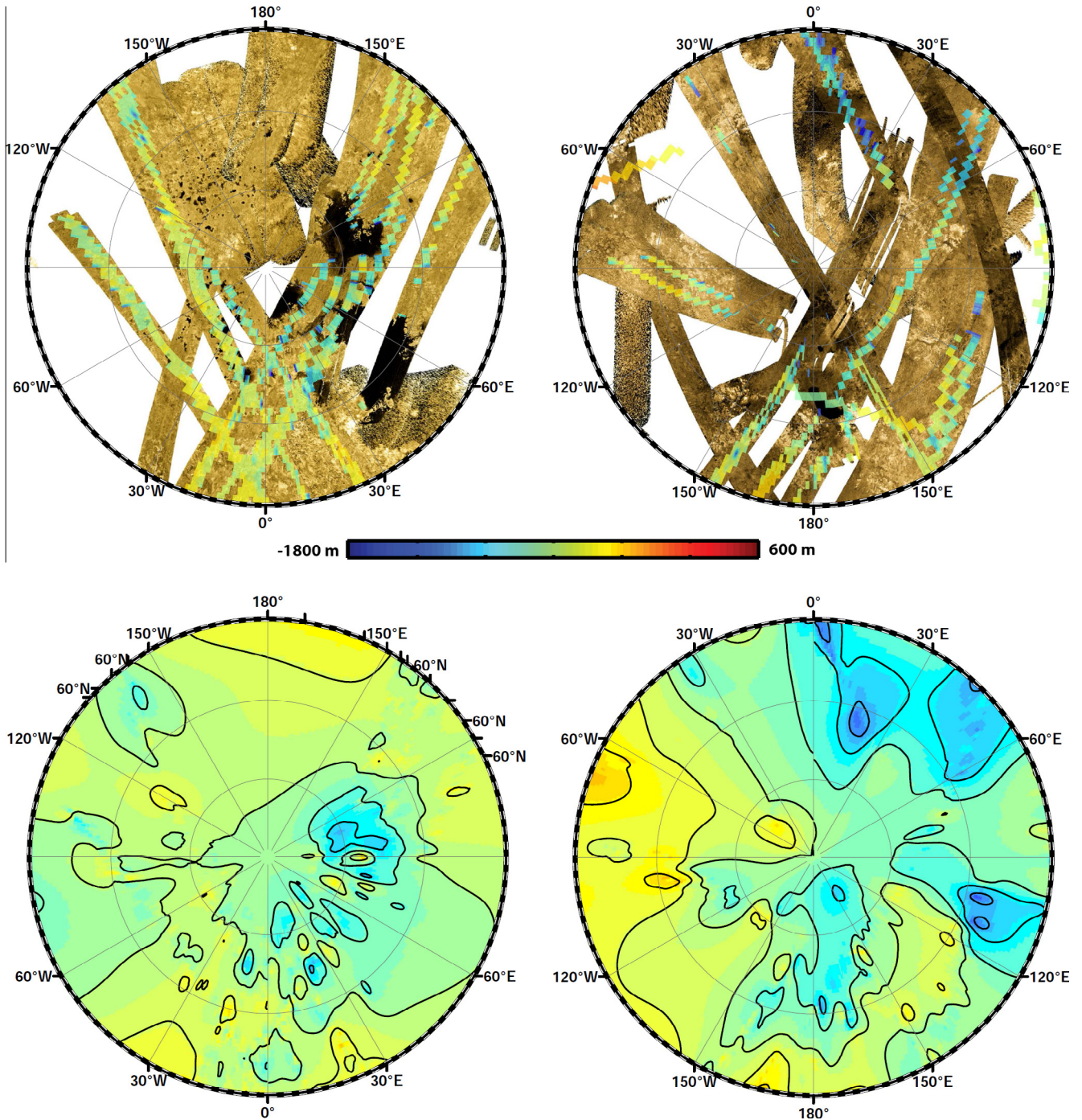


**Fig. 10.** Polar topography maps (bottomleft north, right, south) in stereographic projection, with VIMS/radar maps (top) for comparison. Note the deep basins at 72°S, 340°W and the wider basin at 68°S, 255°W. Ontario Lacus (72°S 183°W) is reassuringly seen to be in a depression, but it is notable that it is by far not the lowest area. Arrakis Planitia (80°S, 120°W) is also found within a local depression. Contour lines are at 200 m intervals.

when humans were migrating out of Africa for the first time, Titan’s arctic may have been somewhat dry and large seas may have been present in the south.

The topographic data presently in hand points to the lowest point being at 59°S, 317°W. It can be seen (Fig. 10) by comparing the topography nearby that if a sea were present here in a previous epoch with a spatial extent (~400 km) comparable with present-day Ligeia Mare, this sea would have a central depth approaching 1000 m.

It is notable that the wettest known place in the south (Ontario Lacus, 79°S, 180°W) is not the lowest place – evidently the entire

southern polar region is not efficiently connected hydraulically (cf. Hayes et al., 2008) and the present liquid in Ontario must have been somewhat locally precipitated. Transient liquids were observed at Arrakis Planitia, 80°S and 120°W (Turtle et al., 2009; Hayes et al., 2011). Both Ontario and Arrakis are in local topographic lows.

#### 4.3. Fluvial networks

The river channels of Elivagar Flumina drain to the northeast (Lorenz et al., 2008) from near the Menrva impact structure at

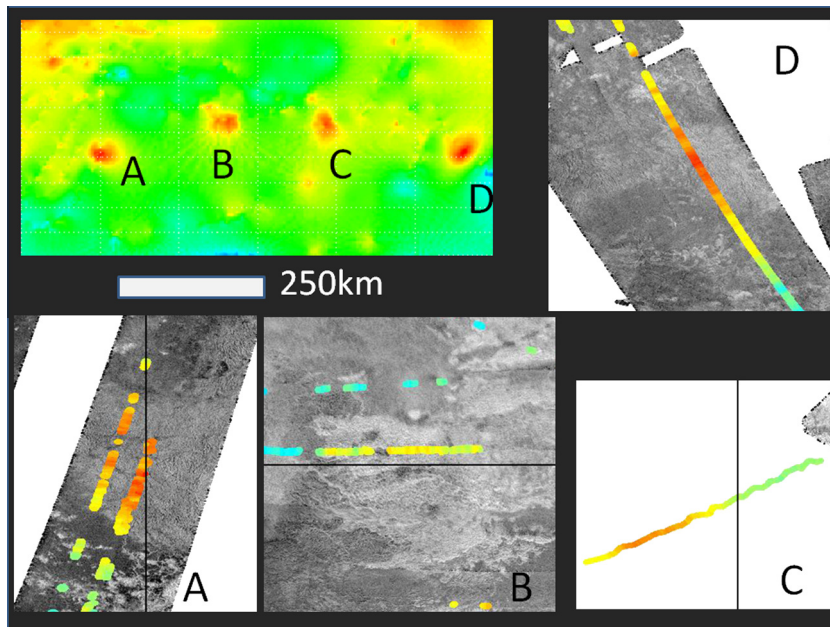


**Fig. 11.** Upper left is a cylindrical projection of the southeast quadrant of the topography map, highlighting four major topographic rises A–D. The insets show SAR images at 1.3 km/pixel with the original SARTopo or altimetry datapoints overlain. In each case seen (A, B and D) the highland terrain is radar-bright and heavily dissected by fluvial valleys. C is only observed in altimetry at present.

20°N, 77°W. (Menrva itself has relatively subdued topography, typical of a crater of its size (Neish et al., 2013), and hence is not observed in the global topographic map.) The topography map here has something of a discontinuity in that the terrain slopes downwards both north and south of the SARTopo tracks from the T3 fly-by that first imaged Menrva and Elivagar. The northeast drainage of Elivagar is consistent with the local topography, which suggests a drop of ~200 m in elevation over ~200 km in that direction.

Other river channels have been identified (e.g. Burr et al., 2009; Lorenz et al., 2008) in Xanadu at around 10S and 125–145°W, draining south. Although the very rugged terrain of Xanadu (Radebaugh et al., 2011) means topography measurements (which could trigger on local mountains) must be interpreted with care, if we take the sensed topography as corresponding to valley-floor elevations, it is reassuring that the topography map indeed shows a southward slope in this area, with in fact a slope of around double that indicated for Elivagar above. This slope difference may be connected with the more incised and developed network in Xanadu compared with the apparently shallow and anabranching/braided arrangement in Elivagar.

#### 4.4. Plateaus

Isolated mountains and mountain belts on Titan seen in SAR imaging have been discussed previously (e.g. Mitri et al., 2010). A striking discovery in the southeastern quadrant of the topography map (see Fig. 11) is an arc of four prominent topographic rises, labeled A, B, C and D. Each is about 200 km wide and stands ~700 m higher than the surrounding terrain. Inspection of the SAR images with the raw topography data overlain for A, B and D shows that the highland terrain is radar-bright and heavily dissected by fluvial valleys. C is only observed in altimetry at present. A, B, and C occur on or near areas that are seen to be darker at 940-nm (Fig. 4). The coordinates and elevations above the 2575 km datum are: A 49°S, 150°W, 380 m; B 35°S, 100°W, 240 m; C 36°S, 63°W, 260 m; D 48°S, 12°W, 350 m. The arrangement of these features draws the eye, but it is unclear if there is any global tectonic relationship between them. Note that some arc-shaped features are apparent in

the upper left quadrant of the map product: these are a result of real data – they correspond to short-wavelength variations between the topography in swaths TA and T3 – so ‘artifacts’ is perhaps not quite an accurate term. However, the arc-shaped arrangement of the plateaus A, B, C and D was not produced in the same way – each feature was observed in a different data take.

## 5. Conclusions

A topographic map has been assembled and interpolated from available Cassini radar data using splining with appropriate regridding around the poles. This map is made available to the community as a gridded dataset for correlative and other studies. Notable features are the overall anticorrelation between elevated terrain and optically dark terrain (contrary to what has been observed at smaller scales), prominent depressions in the south polar regions that may be relict seabeds, the slopes driving large-scale river systems, and the presence of four isolated highland features in southern mid-latitudes.

## Acknowledgments

This work was supported by the Cassini/Huygens mission, which is a joint endeavor of NASA, the European Space Agency (ESA), and the Italian Space Agency (ASI) and is managed by JPL/Caltech under a contract with NASA. RL was supported by NASA Grant NNX13AH14G.

## Appendix A. Supplementary material

Supplementary data associated with this article can be found, in the online version, at <http://dx.doi.org/10.1016/j.icarus.2013.04.002>.

## References

- Aharonson, O., Zuber, M.T., Rothman, D.H., 2001. Statistics of Mars' topography from the Mars orbiter laser altimeter: Slopes, correlations, and physical models. *J. Geophys. Res.* 106, 23723–23735.
- Aharonson, O., Hayes, A., Lunine, J.I., Lorenz, R.D., Elachi, C., 2009. An asymmetric distribution of lakes on Titan as a possible consequence of orbital forcing. *Nat. Geosci.* 2, 851–854.
- Barnes, J.W., Bow, J., Schwartz, J., Brown, R.H., Soderblom, J.M., Hayes, A.G., Vixie, G., Le Moulec, S., Rodriguez, S., Sotin, C., Jaumann, R., Stepha, K., Soderblom, L.A., Clark, R.N., Buratti, B.J., Baines, K.H., Nicholson, P.D., 2011. Organic sedimentary deposits in Titan's dry lakebeds: Probable evaporites. *Icarus* 216, 136–140.
- Brown, R.H., Barnes, J.W., Melosh, H.J., 2011. On Titan's Xanadu region. *Icarus* 214, 556–560.
- Burr, D.M., Jacobsen, R.E., Roth, D.L., Phillips, C.B., Mitchell, K.L., Viola, D., 2009. Fluvial network analysis on Titan: Evidence for subsurface structures and west-to-east wind flow, southwestern Xanadu. *Geophys. Res. Lett.* 36, L22203. <http://dx.doi.org/10.1029/2009GL040909>.
- Hayes, A. et al., 2008. Hydrocarbon lakes on Titan: Distribution and interaction with a Porous Regolith. *Geophys. Res. Lett.* 35, L09204. <http://dx.doi.org/10.1029/2008GL033409>.
- Hayes, A.G., Aharonson, O., Lunine, J., Kirk, R., Zebker, H., Wye, L., Lorenz, R., Turtle, E., Pail lou, P., Mitri, G., Wall, S., Stofan, E.R., Elachi, C. The Cassini RADAR Team, 2011. Transient surface liquid on Titan from Cassini. *Icarus* 211, 655–671.
- Iess, L., Rappaport, N., Jacobson, R.A., Racioppa, P., Stevenson, D.J., Tortora, P., Armstrong, J.W., Asmar, S.W., 2010. Gravity Field, Shape, and Moment of Inertia of Titan. *Science* 327, 1367–1369.
- Larsson, R., Mckay, C.P., 2013. Timescale for oceans in the past of Titan. *Planetary and Space Science* 78, 22–24.
- Lopes, R.M.C. et al., 2013. Cryovolcanism on Titan: New results from Cassini RADAR and VIMS. *J. Geophys. Res. Planets* 118, 1–20. <http://dx.doi.org/10.1002/jgre.20062>.
- Lorenz, R.D., 1996. Characterization of a planet: Dependence on coverage fraction. 27th Lunar Planet. Sci., Houston, TX, March 1996, 773–774.
- Lorenz, R.D., Radebaugh, J., 2009. Global pattern of Titan's dunes: Radar survey from the Cassini prime mission. *Geophys. Res. Lett.* 36, L03202. <http://dx.doi.org/10.1029/2008GL036850>.
- Lorenz, R.D. et al., 2008. Fluvial channels on Titan: Initial Cassini RADAR observations. *Planet. Space Sci.* 56, 1132–1144.
- Lorenz, R.D., Turtle, E.P., Stiles, B., Le Gall, A., Hayes, A., Aharonson, O., Wood, C.A., Stofan, E., Kirk, R., 2011. Hypsometry of Titan. *Icarus* 211, 699–706.
- Mitri, G. et al., 2010. Mountains on Titan: Modeling and observations. *J. Geophys. Res.* 115. <http://dx.doi.org/10.1029/2010JE003592>, CiteID E10002.
- Moore, J.M., Howard, A.D., 2010. Are the basins of Titan's Tui Regio and Hotei Regio sites of former low latitude seas? *Geophys. Res. Lett.* 37, L22205. <http://dx.doi.org/10.1029/2010GL045234>.
- Neish, C.D., Kirk, R.L., Lorenz, R.D., Bray, V.J., Schenk, P., Stiles, B., Turtle, E., Mitchell, K., Hayes, A. the Cassini RADAR Team, 2013. Crater topography on Titan: Implications for landscape evolution. *Icarus* 223, 82–90.
- Nimmoo, F., Bills, B.G., 2010. Shell thickness variations and the long-wavelength topography of Titan. *Icarus* 208, 896–904.
- Radebaugh, J., Lorenz, R.D., Wall, S.D., Kirk, R.L., Wood, C.A., Lunine, J.I., Stofan, E.R., Lopes, R.M.C., Valora, P., Farr, T.G., Hayes, A., Stiles, B., Mitri, G., Zebker, H., Janssen, M., Wye, L., Legall, A., Mitchell, K.L., Paganelli, F., West, R.D., Schaller, E.L. the Cassini RADAR Team, 2011. Regional geomorphology and history of Titan's Xanadu province. *Icarus* 211, 672–685.
- Smith, W.H.F., Wessel, P., 1990. Gridding with continuous curvature splines in tension. *Geophysics* 55, 293–305.
- Smith, D.E., Zuber, M.T., 1996. The shape of Mars and the topographic signature of the hemispheric dichotomy. *Science* 271, 184–188.
- Stiles, B.W., Hensley, S., Gim, Y., Bates, D.M., Kirk, R.L., Hayes, A., Radebaugh, J., Lorenz, R.D., Mitchell, K.L., Callahan, P.S., Zebker, H., Johnson, W.T.K., Wall, S.D., Lunine, J.I., Wood, C.A., Janssen, M., Pelletier, F., West, R.D., Veeramacheni, C. the Cassini RADAR Team, 2009. Determining Titan surface topography from Cassini SAR data. *Icarus* 202, 584–598.
- Stofan, E.R. et al., 2012. Searching for the Remnants of Southern Seas: Cassini Observations of the South Pole of Titan. American Astronomical Society, DPS Meeting #44, #201.08.
- Tokano, T., 2010. Relevance of fast westerlies at equinox for the eastward elongation of Titan's dunes. *Aeolian Res.* 2, 113–127.
- Turtle, E.P. et al., 2009. Cassini imaging of Titan's high-latitude lakes, clouds, and south-polar surface changes. *Geophys. Res. Lett.* 36, L02204. <http://dx.doi.org/10.1029/2008GL036186>.
- Wall, S.D. et al., 2009. Cassini RADAR images at Hotei Arcus and western Xanadu, Titan: Evidence for geologically recent cryovolcanic activity. *Geophys. Res. Lett.* 36, L04203. <http://dx.doi.org/10.1029/2008GL036415>.
- Wye, L., Zebker, H., Lorenz, R., 2009. Smoothness of Titan's Ontario Lacus: Constraints from Cassini RADAR Specular Reflection Data. *Geophys. Res. Lett.* 36, L16201. <http://dx.doi.org/10.1029/2009GL039588>.
- Zebker, H.A., Stiles, B., Hensley, S., Lorenz, R., Kirk, R.L., Lunine, J., 2009a. Size and shape of Saturn's moon Titan from Cassini Radar altimeter and SAR monopulse observations. *Science* 324, 921–923.
- Zebker, H.A., Gim, Y., Callahan, P., Hensley, S., Lorenz, R. the Cassini Radar Team, 2009b. Analysis and interpretation of Cassini Titan Radar Altimeter echoes. *Icarus* 200, 240–255.